

# Modelling and finite element treatment of intra-ply shearing of woven fabric

Xiaobo Yu<sup>a</sup>, Liangchi Zhang<sup>a</sup>, Yiu-Wing Mai<sup>a,b,\*</sup>

<sup>a</sup>*Department of Mechanical and Mechatronic Engineering, Centre for Advanced Materials Technology (CAMT), The University of Sydney, Sydney, NSW 2006, Australia*

<sup>b</sup>*MEEM, City University of Hong Kong, Tat Chee Avenue, Kowloon, Hong Kong*

## Abstract

Diaphragm forming of fibre/epoxy materials is a potential cost-effective approach in manufacturing aerospace components. Significant intra-ply shearing is essential in diaphragm forming a double-curvature geometry. In previous studies, the intra-ply shearing was addressed based on an ideal fibre reinforced fluid (IFRF) model. The IFRF model was tried in the present study for a thermoset material. However, it fails to interpret the experimental results. New models, namely general hinge model and restrained membrane model were thus suggested for intra-ply shearing simulations. The concept of the restrained membrane model was demonstrated using finite element simulations with determined material properties. The proposed model provided a good reproduction of the experimental results. Discussions were given on inherent limitations of the IFRF model and the effects of fibre in-plane bending.

© 2003 Elsevier Science B.V. All rights reserved.

*Keywords:* Diaphragm forming; Intra-ply shearing; Modelling; Finite element simulation

## 1. Introduction

Diaphragm forming of fibre/epoxy materials is a potential cost-effective approach in manufacturing aerospace components. In Australia, the approach has been studied by the CRC-ACS since 1994. Over a 100 experimental trials were conducted on geometric and real components. In brief, a typical double-diaphragm forming process can be described by three steps [1] as schematically illustrated in Fig. 1. In the first step, a flat fabric or tape stack (called a preform) is laid up according to the laminate design, and is placed between two plastic diaphragms. The diaphragms are then secured over the forming box and full vacuum is applied to the cavity between two diaphragms. The second step is to heat up the preform to an appropriate forming temperature. This step applies when pre-impregnated fabric/tape is used. The final step is to evacuate the air volume within the forming box at a controlled rate. Because the air pressure within the forming box becomes smaller than the atmosphere air pressure, the diaphragms deflect and bring down the fabric/tape stack to

conform to the tool geometry. At the end of the process, the formed part is suitable for preparation for autoclave cure.

The diaphragm forming process involves a number of deformation mechanisms [2–4]. For woven fabrics, the predominant mechanisms are intra-ply shearing, in-plane fibre bending, out-of-plane fibre bending, inter-ply sliding and inter-ply rotation (Fig. 2). Significant intra-ply shearing is essential in forming a double-curvature geometry. Previous studies [1,5–10], addressed the intra-ply shearing based on an ideal fibre reinforced fluid (IFRF) model [11], which treats the composite as a continuum of inextensible fibres within a purely viscous or viscoelastic matrix. As shown by Johnson and Costalas [6], the IFRF model provided a reasonable data fitting on the bias tension test results of fabric reinforced thermoplastic prepreg sheets but the micro-mechanism of intra-ply shearing was rarely reflected. In comparison with matrix viscosities, the viscosity values determined by the IFRF model were 2–3 orders larger and showed different rate and temperature dependence.

The present study concerns a woven fabric reinforced thermoset material. The IFRF model was tried; however, it failed to fit the experimental results. An improved modelling on intra-ply shearing was thus proposed and was applied to bias tension simulations with finite element method (FEM). The approach of FEM input data determination is demonstrated.

\* Corresponding author. Present address: Department of Mechanical and Mechatronic Engineering, Centre for Advanced Materials Technology (CAMT), The University of Sydney, Sydney, NSW 2006, Australia.  
Tel.: +61-2-9351-8608; fax: +61-2-9351-3760.  
E-mail address: mai@aeromech.usyd.edu.au (Y.-W. Mai).

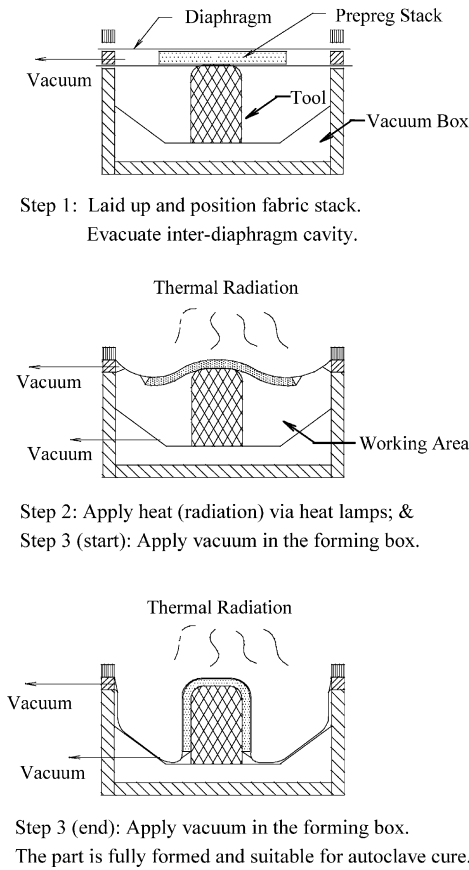


Fig. 1. Schematic illustrations of the double-diaphragm forming process (after [1]).

## 2. Trials with the IFRF model

A number of mutations exist for the IFRF model. The basic forms are to treat the matrix as a purely viscous fluid. For uni-directional fibre reinforced composites, two parameters are needed to describe the longitudinal and transverse viscosities, respectively [5]. For fabric reinforced composites, a complete description requires three independent viscosity parameters [5–7]. However, a simplified one-parameter form can be deduced when the fibre–matrix interaction is ignored, that is, by assuming a constrained viscous fluid [7]. The viscosity parameters in these models can either have a constant value or rate dependencies with power law or cross equation relationships [10].

The pure viscous fluid models do not predict the intra-ply shearing stiffness at zero strain rate. Modifications were therefore introduced by overlaying a linear elastic material on the viscous fluid [10]. As a result, the matrix was simulated by a viscoelastic material.

In the present trials, the IFRF model was further modified by overlaying a rigid–plastic-hardening material on the viscous fluid. Experimental data [12] shows that a rigid–plastic-hardening material is more appropriate than a linear elastic one to simulate the rate-independent intra-ply shearing stiffness. By assuming isotropic viscosity with power

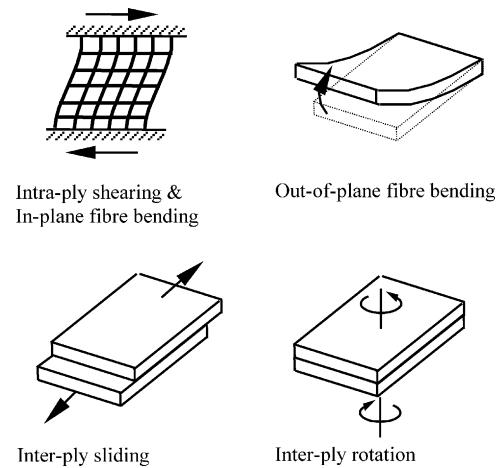


Fig. 2. Predominant intra-ply and inter-ply deformation mechanisms in diaphragm forming process.

law rate dependence, the constitutive relationship for the matrix can be written as

$$s_{ij} = 2\eta_0 \dot{\epsilon}_{ij}^{n-1} \dot{\epsilon}_{ij} + \frac{2}{3} \sigma_s \dot{\epsilon}^{-1} \dot{\epsilon}_{ij} \quad (1)$$

where  $s_{ij}$  and  $\dot{\epsilon}_{ij}$  are deviatoric stress and strain rate, respectively;  $\eta_0$  and  $n$  the parameters for power law viscosity;  $\sigma_s$  the von Mises equivalent stress for rigid–plastic material;  $\dot{\epsilon}$  the equivalent strain rate defined by

$$\dot{\epsilon} = \sqrt{\frac{2}{3} \dot{\epsilon}_{ij} \dot{\epsilon}_{ij}} \quad (2)$$

Consider a bias tension test as shown in Fig. 3(a). Assume that the fibre is inextensible and the matrix is incompressible. If one ignores the fibre in-plane bending stiffness, the tensile force versus matrix stress relationship can be deduced by means of the virtual work principle:

$$\begin{aligned} Fv &= \left[ \left(1 - \frac{3}{2}\lambda\right) \sigma_{ijI} \dot{\epsilon}_{ijI} + \lambda \sigma_{ijII} \dot{\epsilon}_{ijII} \right] L_0 w_0 t_0 \\ &= \left[ \left(1 - \frac{3}{2}\lambda\right) (3\eta_0 \dot{\epsilon}_I^n + \sigma_{sI}) \dot{\epsilon}_I + \lambda (3\eta_0 \dot{\epsilon}_{II}^n + \sigma_{sII}) \dot{\epsilon}_{II} \right] L_0 w_0 t_0 \end{aligned} \quad (3)$$

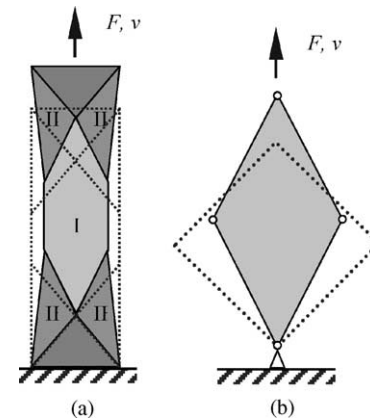


Fig. 3. Deformation profiles of woven fabric under (a) bias tension; (b) picture frame test. At initial state (shown by dotted line), the fibres are along  $\pm 45^\circ$  against the loading direction.

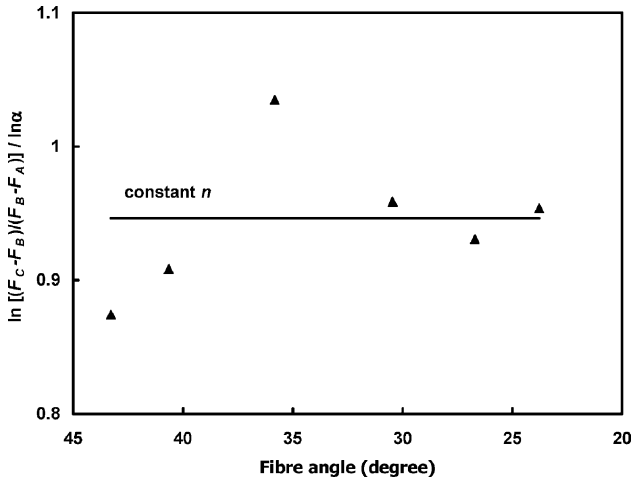


Fig. 4. Determination of power law viscosity index from experimental data.

where  $\lambda = w_0/L_0$ ;  $L_0$ ,  $w_0$  and  $t_0$  the original length, width and thickness of the fabric sheet, respectively;  $\sigma_{ijI}$ ,  $\dot{\epsilon}_{ijI}$  and  $\sigma_{ijII}$ ,  $\dot{\epsilon}_{ijII}$  the stress and strain rate components over zones I and II, respectively;  $\sigma_{sI}$ ,  $\dot{\epsilon}_I$  and  $\sigma_{sII}$ ,  $\dot{\epsilon}_{II}$  the von Mises equivalent stresses (for rigid–plastic material) and equivalent strain rates over zones I and II, respectively.

In the case that three tests were performed with loading speeds of  $v_0$ ,  $\alpha v_0$  and  $\alpha^2 v_0$ , the index of the power law viscosity can be determined by the following equation:

$$\frac{F_C - F_B}{F_B - F_A} = \alpha^n \quad (4)$$

where  $F_A$ ,  $F_B$  and  $F_C$  are the tensile forces corresponding to  $v_0$ ,  $\alpha v_0$  and  $\alpha^2 v_0$  loading speeds, respectively. When  $n$  is determined,  $\eta_0$  can be found out by taking  $(F_B - F_A)$  and  $(F_C - F_B)$  based on Eq. (3). Thereafter the  $\sigma_s$  versus  $\epsilon$  relationship is simply deduced from Eq. (3).

The above approach was tested against the test results provided in Ref. [13]. Fig. 4 shows the power law viscosity

index determination based on Eq. (4). It is clear that the experimental data cannot be fitted by a constant  $n$  value. Larger scatters were observed in  $\eta_0$  and  $\sigma_s$ .

Fig. 5 compares the experimental data and the model predictions of the tensile force for the bias tension test. The predictions were based on optimised values of  $n$ ,  $\eta_0$  and  $\sigma_s$ . Obviously, the IFRF model does not apply to the present case and improved modelling is needed for better simulation.

### 3. The proposed model for intra-ply shearing stiffness

Although not unequivocally confirmed, the intra-ply shearing stiffness of a fabric sheet most likely comes from the fibre-to-fibre and fibre-to-matrix frictions. This means that the composite viscosity is an equivalent viscosity of the fibre–matrix structure rather than the viscosity of the matrix material. To reflect this feature, the constitutive relationship of an intra-ply shearing model will have a general form as

intra-ply shearing stiffness

$$= f(\text{deformation rate, fibre–matrix structure}) \quad (5)$$

When the in-plane deformation profile is dominated by trellis deformation, the fibre angle  $\theta$  or equivalent strain  $\epsilon$  provides a unique index of the fibre–matrix structure for a given fabric.

Fig. 6 illustrates two possible intra-ply shearing models that can be implemented into FEM simulations.

For general hinge model, an elasto-plastic hinge is used to simulate the intra-ply shearing stiffness. The constitutive relationship of the hinge can be written as

$$M = f_M(\dot{\theta}, \theta) \quad (7)$$

where  $M$  is the in-plane moment against fibre angle change. For restrained membrane model, the intra-ply shearing

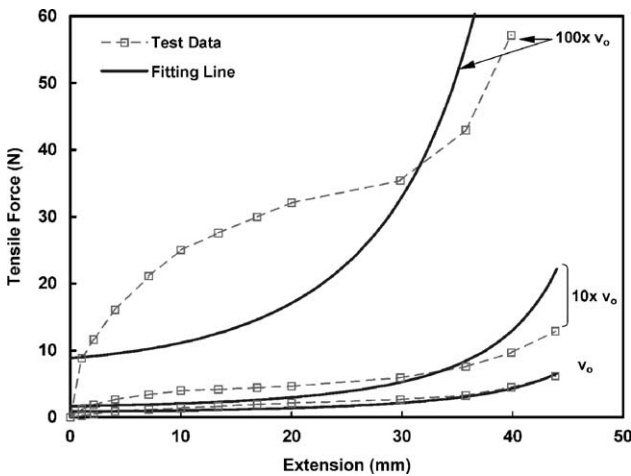


Fig. 5. Tensile forces in bias tension tests. Comparison between experimental data and the IFRF model predictions.

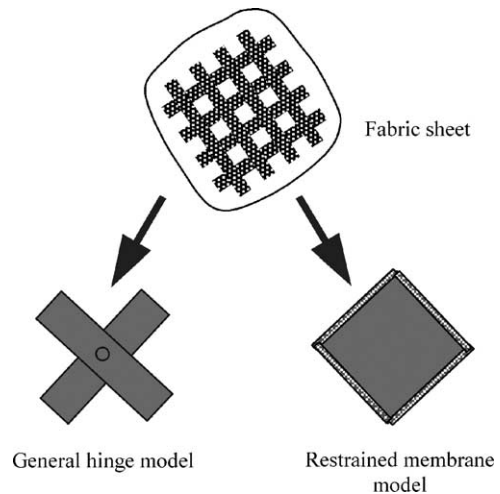


Fig. 6. Illustrations of intra-ply shearing models for FEM analysis.

stiffness is equivalently described by the isotropic rate-dependent hardening membrane whose deformation profile is constrained by the trellis deformation of the fibres. The constitutive relation for the membrane can be written as

$$\sigma = f_{\sigma}(\dot{\epsilon}, \epsilon) \tag{8}$$

The present study does not attempt to deduce the micro-mechanisms for functions  $f_M$  and  $f_{\sigma}$ . Instead, the constitutive relationships will be determined based on experimental data. Without losing generality, the remaining parts of the paper will focus on the restrained membrane model.

**4. Material property determination for the proposed model**

Picture frame (Fig. 3b) and bias tension (Fig. 3a) are two types of tests commonly used for measuring intra-ply shearing stiffness. For picture frame test, the  $\sigma$ - $\epsilon$ - $v$  relationship can be directly solved from the following equation based on virtual work principle:

$$Fv = \sigma \dot{\epsilon} A_0 t_0 \tag{9}$$

where  $A_0$  and  $t_0$  are the original area and thickness of the fabric sheet, respectively. Following an interpolation procedure against  $\dot{\epsilon}$ , the  $\sigma$ - $\epsilon$ - $v$  relationship can be converted into a  $\sigma$ - $\epsilon$ - $\dot{\epsilon}$  relationship, so that the material properties for the restrained membrane are obtained.

For the bias tension test, Eq. (3) still applies except the second equator. Because both  $\sigma_I$  and  $\sigma_{II}$  are unknown, an iteration approach as illustrated in Fig. 7 is suggested. Using the same experimental data as used in Section 2 (trials with the IFRF model), Fig. 8 shows that the iteration procedure converges quite quickly. Fig. 9 plots the material properties obtained at the end of the 10th iteration.

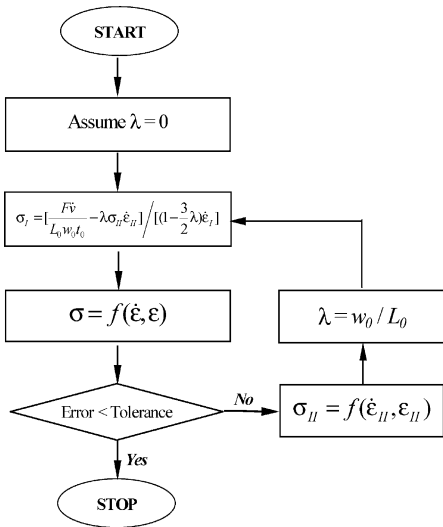


Fig. 7. A flow chart showing iteration approach to determine material properties from bias tension tests.

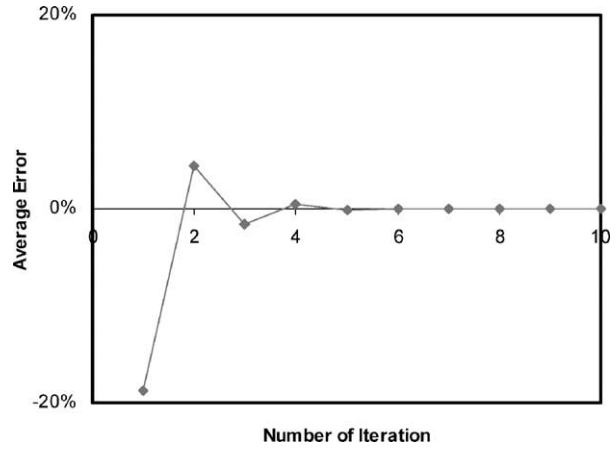


Fig. 8. The convergence of material property determination by the iteration approach.

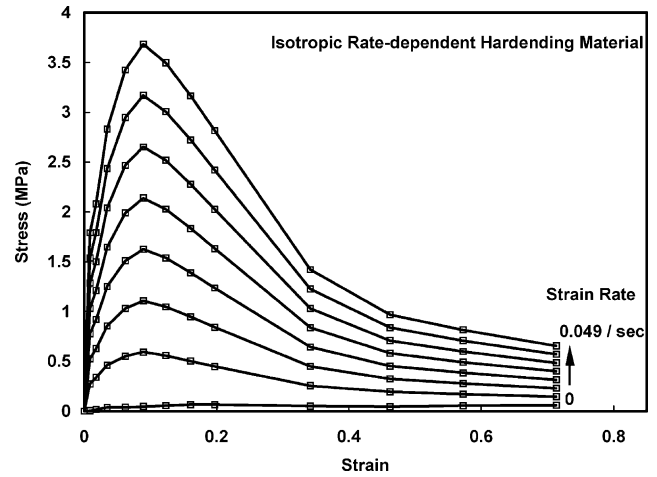


Fig. 9. The material properties of restrained membrane for equivalent simulations of intra-ply shearing stiffness.

**5. FEM simulations on bias tension tests**

ABAQUS/Explicit 5.8 was used for FEM simulations. The fibres were simulated by linear elastic truss/beam elements. The intra-ply shearing stiffness was simulated by membrane elements with material properties as shown in Fig. 9. The fibre in-plane bending stiffness was ignored for the moment.

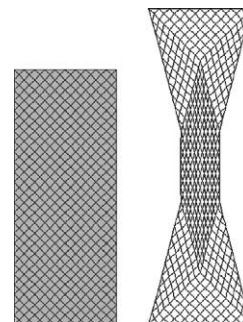


Fig. 10. Initial and deformed mesh profiles in bias tension test simulations.

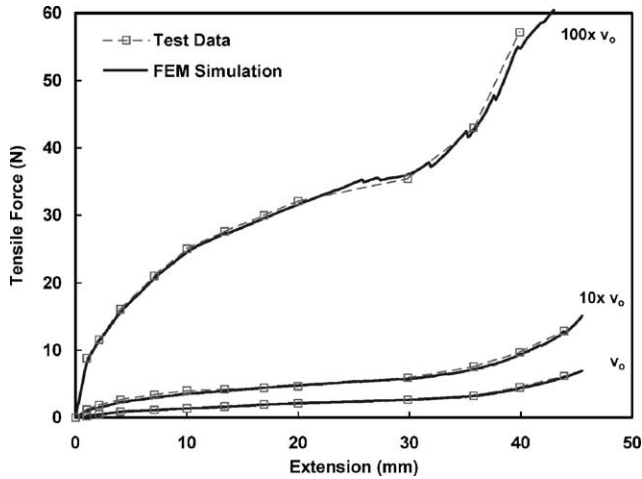


Fig. 11. Tensile forces in bias tension tests. Comparison between experimental data and FEM predictions based on the restrained membrane model.

The initial and deformed meshes of the fabric sheet are shown in Fig. 10. The edges of the elements coincide with the fibre orientations. Fig. 11 is a comparison of the experimental data and FEM simulations. It shows that the proposed modelling provides a good reproduction of the experimental results.

### 6. Discussion

In the present study, two models have been examined for the intra-ply shearing stiffness simulation: one is an IFRF model, the other is the proposed restrained membrane model. The proposed model yields a much better simulation of the experimental data. To further examine the models, the constitutive relationship of the IFRF model, Eq. (1), is plotted in Fig. 12 in a  $\sigma-\varepsilon-\dot{\varepsilon}$  format. It can be seen that the vertical distances between any two curves in the figure do not change with the strain value. This is a feature associated

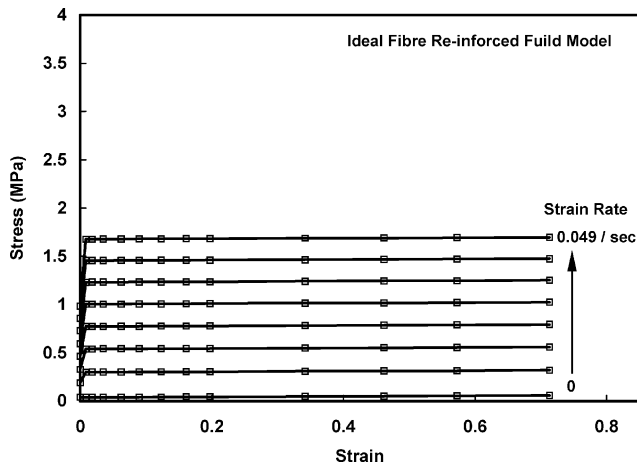


Fig. 12. The material properties based on the IFRF model with isotropic power law viscosity.

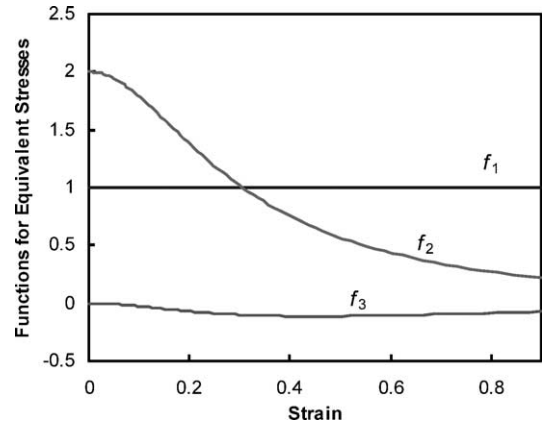


Fig. 13. Functions used to calculate equivalent von Mises stresses for an IFRF model with anisotropic viscous fluid.

with the isotropic viscosity assumption. There are no combinations of  $\eta_0, n$  and  $\sigma_s$  that can tune the curves in Fig. 12 to the shape posed in Fig. 9. Therefore, an accurate simulation can never be achieved by this IFRF model.

It may be argued that the isotropic viscosity is just a special case of the anisotropic viscosity that has three independent viscosity parameters. For intra-ply shearing, the equivalent viscosity,  $\eta^*$ , can be written as [7]:

$$\eta^* = \eta_1 + 2\eta_2 \frac{\sin^2 2\theta}{4 - 3 \sin^2 2\theta} - \frac{1}{4} \eta_3 \frac{\sin^2 4\theta}{4 - 3 \sin^2 2\theta} \quad (10)$$

Based on Eq. (10), the equivalent von Mises stress for the viscous fluid can be written as

$$\sigma_s = 3(\eta_1 f_1 + \eta_2 f_2 + \eta_3 f_3) \dot{\varepsilon} \quad (11)$$

where  $f_1, f_2, f_3$  are functions plotted in Fig. 13. Obviously, if the material properties of the IFRF model are plotted in a  $\sigma-\varepsilon-\dot{\varepsilon}$  format, the  $\sigma$  distance between two  $\sigma-\varepsilon$  curves (with different  $\dot{\varepsilon}$ ) will no longer keep constant along the  $\varepsilon$  axis. However, a careful examination of Fig. 13 shows no combinations of  $\eta_1, \eta_2$  and  $\eta_3$  that can tune the curves into the shape given in Fig. 9. Therefore an accurate simulation is still not available.

The problem with the IFRF model is actually caused by the inherent assumption of the viscous fluid. It was known that the IFRF model did not reflect the micro-mechanisms of intra-ply shearing and was only used to provide some kinds of equivalent descriptions [6]. With the viscous fluid assumption, either isotropic or anisotropic, the material properties for an equivalent description are somehow pre-shaped. Therefore, the IFRF model will not have enough freedom to fit the experimental data. In comparison, the proposed model assumes a material with any possible constitutive relationship so that the experimental data can be fully interpreted. Nevertheless, it should be noted that the proposed model will be only useful when the in-plane deformation profile is dominated by trellis deformation.

In addition, it should be noted that the material property determination and the FEM simulation presented in previous

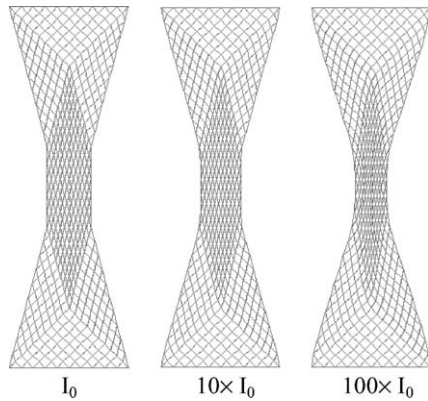


Fig. 14. Effects of fibre in-plane bending stiffness on fabric deformation profile.

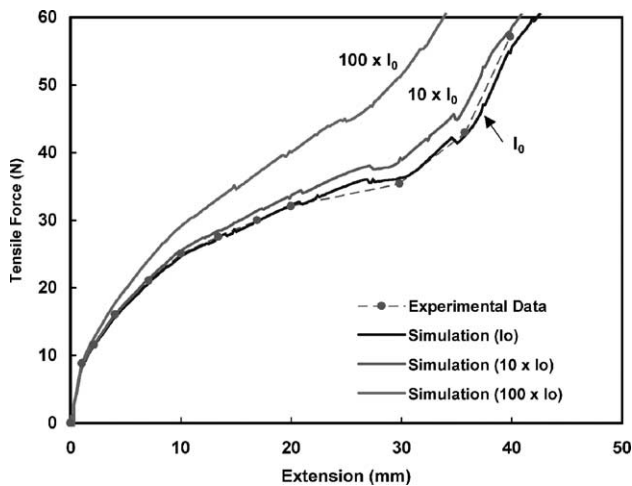


Fig. 15. Effects of fibre in-plane bending stiffness on simulated tensile forces.

sections only apply when the fibre in-plane bending stiffness is ignored. As shown in Figs. 14 and 15, the fibre in-plane bending stiffness does affect the fabric sheet deformation profile as well as the tensile forces. Further studies are needed in this area.

## 7. Conclusions

- (1) It is known that the IFRF model does not reflect the micro-mechanism of the intra-ply shearing of a fabric sheet. The present study further shows that it does not provide a reasonable interpretation of experimental data at the macro-mechanical level. The problem with the IFRF model can be attributed to the inherent assumption of a viscous fluid.
- (2) The present study proposed and demonstrated a restrained membrane model for intra-ply shearing

simulations. The model can be implemented by FEM simulation with an explicit solution method. It provides a good description of the experimental results.

- (3) The material input data can be determined based on the proposed approach.
- (4) To finalise the proposed model, future study on fibre in-plane bending stiffness effects is needed.

## Acknowledgements

This work was carried out as part of the research program of the Cooperative Research Centre for Advanced Composite Structures (CRC-ACS).

## References

- [1] X. Yu, B.K. Cartwright, L. Zhang, R. Paton, Y.-M. Mai, Finite element simulations of the diaphragm forming process, in: Proceedings of the 15th Annual Technical Conference of the American Society for Composite, September 24–27, 2000, Texas, USA.
- [2] F.N. Cogswell, The processing science of thermoplastic structural composites, *Int. Polym. Process.* 1 (4) (1987) 157–165.
- [3] C.M. O'Brádaigh, R.B. Pipes, P.J. Mallon, Issues in diaphragm forming of continuous fibre reinforced thermoplastic composites, *Polym. Compos.* 12 (4) (1991) 246–258.
- [4] O.K. Bergsma, Computer simulation of 3D forming processes of fabric reinforced plastics, in: Proceedings of the ICCM-9, Composites Design, 1993.
- [5] T.G. Rogers, Rheological characterization of anisotropic materials, *Composites* 20 (1) (1989) 21–27.
- [6] A.F. Johnson, E. Costalas, Forming models for fabric reinforced thermoplastics, in: Proceedings of the Fourth International Conference on Automated Composites (ICAC'95), Nottingham, UK, 1995.
- [7] A.F. Johnson, Rheological model for the forming of fabric-reinforced thermoplastic sheets, *Compos. Manuf.* 6 (1995) 153–160.
- [8] P. De Luca, et al., Development validation and first industrial numerical results of a finite element code to simulate the thermoforming process, in: Proceedings of the Fourth International Conference on Automated Composites (ICAC'95), Nottingham, UK, 1995.
- [9] A.F. Johnson, A.K. Pickett, Numerical simulation of the forming process in long fibre reinforced thermoplastics, in: Proceedings of the Fifth International Conference on Computer Aided Design in Composite Material Technology, Italy, 1996.
- [10] G.B. McGuinness, C.M. O'Brádaigh, Development of rheological models for forming flows and picture-frame shear testing of fabric reinforced thermoplastic sheets, *J. Non-Newton. Fluid Mech.* 73 (1997) 1–28.
- [11] A.J.M. Spencer, *Deformation of Fibre-reinforced Materials*, Clarendon Press, Oxford, 1972.
- [12] J. Wang, J.R. Page, R. Paton, Experimental investigation of the draping properties of reinforcement fabrics, *Compos. Sci. Technol.* 58 (1998) 229–237.
- [13] J. Wang, R. Paton, J.R. Page, Forming properties of thermoset fabric prepreps at room and elevated temperature, CRC-ACS TM 97028, 1997.